3D Modelling of a Solar Thermochemical Reactor for MW Scaling-up Studies

Stylianos Kyrimis[1], Patrick Le Clercq[1, a)] and Stefan Brendelberger[2]

[1]*Institute of Combustion Technology, Deutsches Zentrum für Luft- und Raumfahrt e.V. (DLR), Stuttgart 70569, Germany*
[2]*Institute of Solar Research, Deutsches Zentrum für Luft- und Raumfahrt e.V. (DLR), Köln 51147, Germany*

[a)]Corresponding author: Patrick.LeClercq@dlr.de

Abstract. A lab-scale solar reactor, equipped with a porous CeO_2 structure with dual-scale porosity for CO_2 and H_2O splitting, has been simulated and validated using available experimental results. The validated model was then used to scale-up the geometry to the MW scale and to investigate the benefits in the studied reactor. The larger reactors displayed partially better performance, but their potential was limited by the restricted thickness of the porous structure during scaling-up. This restriction accelerated the temperature uniformity in the CeO_2 volume, followed by saturation and a steady-state effect with reduced O_2 production. The validated model can be used for further reactor optimization, which should be addressed in combination with a dedicated plant design study for continuous carbon-neutral fuel production.

INTRODUCTION

One of the main anthropogenic greenhouse gas emission sources is the transportation sector, which was responsible for approximately 23% of the total energy-related CO_2 emissions in 2010 [1]. The transportation sector will continue to depend on conventional liquid fuels since their high energy density is ideal for the existing infrastructure [2], especially in the case of aviation. The European Union proposed an energy strategy for 2030, with the goal of 40% reduction in greenhouse gas emissions [3] compared to 1990 levels. Therefore, the sustainable production of aviation fuels will prove a substantial contributor to the emission reduction goal, since a complete infrastructure change by 2030 is unlikely. One of the available options for carbon-neutral aviation fuel production is through the production of renewable syngas by splitting CO_2 and H_2O using concentrated solar energy in a solar thermochemical process. The produced syngas is then further processed to hydrocarbons via the well-established Fischer-Tropsch synthesis. The splitting can be achieved under technically relevant conditions by using porous structures made out of redox active metal oxides, such as ceria (CeO_2), which are placed in the cavity-receiver of a solar thermochemical reactor and which are cycled through a reduction step and an oxidation step, as in equations (1) and (2a), (2b), respectively [4,5]:

$$\frac{1}{\delta_{red}-\delta_{ox}}CeO_{2-\delta_{ox}} \rightarrow \frac{1}{\delta_{red}-\delta_{ox}}CeO_{2-\delta_{red}} + \frac{1}{2}O_2 \quad (1)$$

$$\frac{1}{\delta_{red}-\delta_{ox}}CeO_{2-\delta_{red}} + H_2O \rightarrow \frac{1}{\delta_{red}-\delta_{ox}}CeO_{2-\delta_{ox}} + H_2 \quad (2a)$$

$$\frac{1}{\delta_{red}-\delta_{ox}}CeO_{2-\delta_{red}} + CO_2 \rightarrow \frac{1}{\delta_{red}-\delta_{ox}}CeO_{2-\delta_{ox}} + CO \quad (2b)$$

Here δ is the non-stoichiometry of ceria. The reduction step is typically operated at temperatures around 1773-1973 K [5,6]. The high-temperatures necessary for the porous structure to undergo this endothermic step are achieved by exposing the cavity-receiver to concentrated solar radiation. For the exothermic oxidation step, ceria is

cooled down to temperatures in the range of 1273 K - 873 K [5]. Two lab-scale thermochemical reactors have already been designed and tested [5,7]. The first configuration [7], which utilized a Reticulated Porous Ceramic (RPC) with single-scale porosity, has been successfully simulated using 3D CFD and has been validated according to the available experimental results [8,9]. In the second configuration [5], ceria is in the form of a dual-scale RPC which consists of a foam porosity in the mm-scale and a strut porosity in the μm-scale. The dual-scale RPC has been experimentally proven superior than the single-scale RPC [10] and the second reactor configuration achieved a record solar-to-fuel (s-t-f) energy conversion efficiency of 5.25 %, greatly outperforming the first configuration, which was at 1.73%.

Despite the record lab-scale reactor performance, this technology has to be scaled up and achieve a substantial improvement in the solar-to-fuel energy conversion efficiency in order to be economically feasible and contribute to the EU climate goals. The design and operation of a dedicated plant that utilizes the solar reactor technology for continuous fuel production is challenging but it can be greatly accelerated through the use of validated simulation tools that can predict the behavior of larger scale reactors. In the present article, the second reactor configuration will be simulated and validated using the existing experimental results [5]**.** The validated model will then be used to scale-up the geometry to scales relevant in a fuel production plant, equal to 0.3, 1 and 3 MW, and their performance will be assessed using a 3D axisymmetric model.

MODELLING METHODOLOGY

The solar reactor, presented in Marxer *et al.* (2017) [5], consists of a 75 mm deep and 100 mm inner diameter cavity-receiver with a 4 cm-diameter aperture in the front. The cavity contains a 25 mm-thick CeO_2 RPC and is enclosed in the front by a 4 mm-thick quartz window. A layer of Al_2O_3 insulation is placed around the CeO_2 RPC and an aluminum layer in the front face of the reactor acts as a radiation shield. The entire reactor is encased in an Inconel vessel. This geometry, as well as the scaled-up reactors, were all simulated as axisymmetric 3D geometries with a size equal to $1/8^{th}$ of the initial total volume. The smaller volume of the axisymmetric geometry allows the use of a finer mesh, thus leading to higher resolution without the corresponding computation time increase. However, because of the axisymmetric symmetry, buoyancy effects are disabled. The design and meshing of the 3D geometry were done with ANSYS DesignModeller and Meshing, respectively and the 3D simulations were performed using the commercial tool ANSYS CFX R17.1.

The main modelling methodology was established in previous works [8,9]. Only a brief summary is presented in this paper. In the fluid regions within the cavity, the local instantaneous form of the mass, the momentum and the total energy equations are solved [11]. The low velocity of the flow generated by Argon injection and/or pumping outflow is in the order of magnitude 10^{-3}-10^{-4} m/sec, allowing the assumption of laminar flow conditions since the Reynolds number is below the transition threshold for the studied geometries. Thermal radiation was modelled using a Monte-Carlo (MC) approach, with 10^4-10^7 particles, increasing with the reactor scale. In order to focus the parallel MC particle trajectories in the aperture area, a lens domain, modelled as incompressible air with a high refractive index, was implemented in front of the window, similar to [8] and [9]. To ensure uniform radiation distribution within the cavity and on the irradiated surface, a coarsening rate of 4 was used in all cases.

The utilized model in the porous computational domain is a generalization of the Navier-Stokes equations combined with Darcy's law. It is assumed that infinitesimal control volumes and surfaces are large relative to the interfacial spacing of the porous medium but small relative to the resolution scales [11]. The different elements of the simulated porous medium are treated as containing both fluid and solid regions, resulting in the coexistence of two separate phases with significantly different properties. As a result and because the thermal radiation is mainly absorbed by the solid regions, which are thus heated faster than the fluid regions, a non-thermal local equilibrium model is required, established by the use of two separate energy equations, one for the fluid phase, Eq. (3), and one for the solid phase, Eq. (4). The two separate energy equations are coupled with a convective heat transfer term, given in Eq. (5) as Q_{fs}, with its magnitude estimated through the use of the convective heat transfer coefficient, h_{sf}, and the specific surface area, A_{fs}, between the two phases [11, 8, 9]. The incoming thermal radiation, after reaching the RPC surface, is partially absorbed while the remaining is scattered, reflected and emitted in the surroundings and deeper into the pores. Because of the optically thick RPC [8, 9, 12], this deeper penetration can be approximated as a diffusion process, modelled with the Rosseland approximation, by introducing the total radiative conductivity, given in Eq. (6), on the energy equation of the solid phase, given in Eq. (4) [11, 12]:

$$\varepsilon\rho_f Cp_f \frac{\partial T_f}{\partial t} + \left(\varepsilon\rho_f Cp_f\right)\mathbf{U}\cdot\nabla T_f = k_f \nabla\cdot\nabla T_f + Q_{fs} \tag{3}$$

$$(1-\varepsilon)\rho_s Cp_s \frac{\partial T_s}{\partial t} = -(k_s + k_r)\nabla \cdot \nabla T_s + Q_{fs} \quad (4)$$

$$Q_{fs} = h_{sf} A_{fs}(T_s - T_f) \quad (5)$$

$$k_r = -\frac{16\sigma n_{eff}^2 T^3}{3\beta} \quad (6)$$

Here, ε refers to the total volume porosity of the RPC, ρ, Cp and k refer to the density, specific heat capacity and thermal conductivity of the fluid/solid porous parts, considered as Argon and CeO_2 respectively, and k_r is the radiative conductivity, introduced by the Rosseland approximation. In Eq. (6), σ is the Stefan-Boltzmann constant, n_{eff} is the effective refractive index for the dual-scale RPC and β is the extinction coefficient, taken from [5].

The advantages of the dual-scale porosity are deeper radiation penetration, due to the mm-pore scale, combined with improved heat and mass transfer as well as chemical activity, caused by the increased surface area provided by the μm-pore scale [10]. To capture the benefit of the two distinct pore sizes, the use of effective properties is required. The effective heat transfer coefficient, $h_{sf,eff}$, and specific surface area between the fluid and solid regions, $A_{fs,eff}$, are used in the porous computational domain and are estimated through the contribution of each scale:

$$\text{Effective Property} = \frac{\varepsilon_{RPC\text{-}Single}}{\varepsilon}\text{Property}_{mm\text{-}scale} + \frac{(1-\varepsilon_{RPC\text{-}Single})\varepsilon_{Strut}}{\varepsilon}\text{Property}_{\mu m\text{-}scale} \quad (7)$$

Here $\varepsilon_{RPC\text{-}Single}$, ε_{Strut}, and ε are the mm-scale, μm-scale, and total porosity, respectively. Equation (7) was derived from the dual-scale porosity equation presented in Ackermann *et al.* (2017) [6]. To approximate the aforementioned diffusion-like process within the pores, the irradiated interface of the porous computational domain was modeled as opaque as part of the boundary conditions of the radiative heat transfer. The high temperature reached there, due to the intense radiation, will cause an enhanced convective and radiative contribution affecting and being magnified by both pore scales. The combined diffusive and convective heat transfer was accounted for by using the effective heat transfer coefficient, $h_{sf,eff}$, at the opaque interface to estimate the magnitude of the heat transfer effects between the two phases. On the contrary, at the back interface of the porous computational domain, diffusion is exhausted through absorption while convection is minimized due to temperature equilibrium. There, conduction is the dominant heat transfer mechanism and it is assumed that the contribution of the μm-scale pores is negligible for conduction purposes. As a result, the mm-scale heat transfer coefficient, $h_{sf,mm\text{-}scale}$, is used. While this approach, based on a continuous porous domain with effective properties, differs from the one presented in [6], which is based on direct pore-level simulation (DPLS), and there is a 5% deviation in the estimated contribution of the μm-scale pores, it allows the approximation of the higher complexity of the dual-scale structure in the more generalized porous model.

Flow Conditions and Post-Process Analysis

During the simulated reduction step, in order to capture the flow conditions that take place within the cavity, a source of fluid is introduced in each element of the porous domain when its temperature is above 1200 K [10], with the amount of fluid released derived from the experimental production of O_2 [5]. The same value was used to calculate the outflow of the pump, operated to purge the produced fluid and keep a constant pressure within the cavity. As in the experiments, Argon was injected through a small opening at the front side of the cavity. To avoid two separate species in the fluid phase, the fluid released at each source point and flowing out of the cavity is assumed to be a single species, Argon.

The direct implementation of the O_2 chemical release, coupled with the fluid dynamics, is not stable. Therefore, a post processing methodology is used to estimate the O_2 released and thus the solar-to-fuel energy conversion efficiency. The temperature of each ceria element for each minute, over the duration of the reduction step, is extracted and used to calculate the change in the non-stoichiometry, Δδ, through the equation presented in Ackermann *et al.* (2017) [6]. For the calculation, the oxygen partial pressure, P_{O2}, is assumed fixed and equal to one third the initial cavity pressure. The P_{O2} is estimated from the pressure difference reached during the experimental reduction, which is caused by the remnants of O_2 within the cavity [5]. The estimated amount of O_2 is calculated from Eq. (8) [13] and is directly linked to the amount of fuel (here assumed pure CO) produced during the re-oxidation step. From the chemical formulas, Eq. (1) and (2), and assuming full re-oxidation of ceria for every cycle, the amount of CO produced is twice the amount of released O_2 and thus the solar-to-fuel energy conversion efficiency can be calculated from the same formula as in the experimental setup [5]:

$$O_2\ (\text{mol}) = \frac{\Delta\delta}{2}\frac{m_{Ceria}}{M.W._{Ceria}} \tag{8}$$

$$n_{solar\text{-}to\text{-}fuel} = \frac{n_{CO} \cdot \Delta H_{CO}}{Q_{solar} + Q_{pump} + Q_{inert}} \tag{9}$$

Where $M.W._{Ceria}$ is the molar weight of ceria, n_{CO} is the number of moles of CO produced, ΔH_{CO} is the higher heating value of CO, Q_{solar} is the radiative input during reduction and Q_{pump} and Q_{inert} are the energy penalties due to pumping and inert gas consumption, respectively.

MODEL VALIDATION

A single reduction step of the 3.5 kW reactor was simulated. Transient terms are solved using a second order backward Euler, while the advection term uses a high resolution scheme. The pressure within the cavity was fixed at 10 mbar. The radiative input power, measured at the aperture, as well as the flow conditions were all expressed in corresponding axisymmetric values. A steady-state solution, operated until the average RPC temperature was above 800 K, was used as the initial condition for the unsteady computation of the reduction step, corresponding to the state of the reactor at the end of a general oxidation step. Reduction lasted until an average RPC volume temperature of around 1773 K was reached. The available experimental results for the respective geometry, presented in Marxer *et al.* (2017) [5], are used to validate the simulated results. The average volumetric temperature evolution of the RPC, compared to the nominal reactor temperature from [5], is presented in Fig. 1(a). Also shown on the same figure is the estimated and experimental O_2 production rate during reduction. The state of the reactor at the end of the reduction step can be seen in Fig. 1(b).

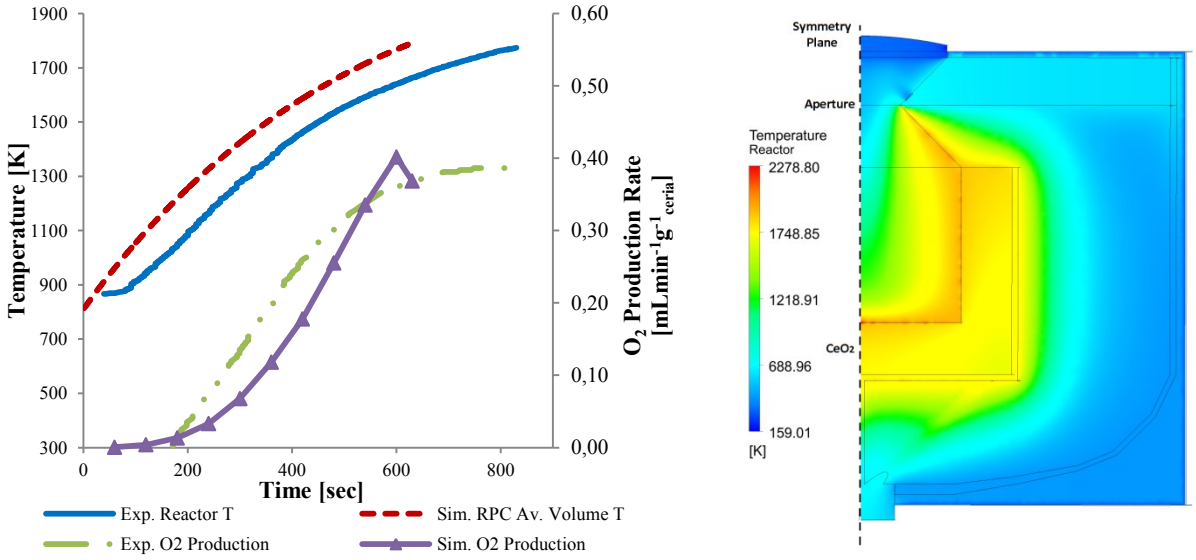

(a) (b)

FIGURE 1. (a) The simulated and experimental [5] temperature and O_2 evolution. (b) The state of the 3.5 kW reactor at the end of the reduction step, which lasted until the RPC volume temperature of 1773 K was reached.

The exposed RPC surface is gradually heated up to an average area temperature of 1892 K after 630 seconds and the resulting end-state temperature difference across the RPC is around 147 K. Part of the incoming radiation is reflected from the ceria surface onto the conical surface of the Al_2O_3 insulation within the cavity, causing it to reach an average temperature of 1925 K at the end of the reduction step. Considering that the maximum operating temperature suggested for Al_2O_3 is around 2073 K [14], continuous daily operation at such high temperatures and with no heat recovery (i.e. cooling) mechanism will cause severe thermal stress and eventually damage the

insulation. The installation of a thin ceria layer in this section would both protect the insulation while also capturing useful heat for O_2 production, since the temperature reached there is high enough to maintain the reduction reaction.

The comparison of the temperature evolution in the RPC, between simulated and experimental results, presents a temperature difference of around 130 K throughout the reduction duration. Furthermore, the simulated case reaches the 1773 K temperature limit much sooner than the experimental case. It is expected that this difference is caused by different reactor temperature measurement strategies: while in the simulation, the average RPC volume temperature can be easily obtained, in the experiment it is expected that the temperatures are rather measured at the back of the RPC. This assumption agrees with the delay in temperature increase at the beginning of the irradiation.

Regarding the O_2 production rate, the experimental O_2 evolution starts sooner and reaches a plateau when the heating rate slows down. On the contrary, the estimated O_2 evolution in the simulation is much slower at the earlier stages but keeps increasing until the completion of the reduction step with a similar rate as the experimental results. The estimated O_2 release is lower than the experimental production, a result which would lead to under-prediction of the s-t-f energy conversion efficiency. Overall this leads to a conservative estimation of the reactor performance.

Despite not achieving a perfect accuracy, the simulation is able to capture correctly the heat and mass transfer, as well as the chemical effects (i.e. O_2 release) that take place during the thermal reduction of ceria. Most importantly, the simulated geometry is able to reproduce the heating up and O_2 production trends and give a realistic depiction of the reactor's behavior during reduction in very acceptable computational times, facts that make simulations a valuable tool for design and scaling-up studies, such as the ones presented in this paper. Accuracy of the simulations could be greatly improved by more precise boundary conditions, temperature measurement location, and improved modelling.

SCALE-UP STUDY

The presented lab-scale geometry has been scaled up to three larger designs, 0.3, 1 and 3 MW, scales that could be relevant in a fuel production plant. There are two important reactor characteristics to consider for scaling-up: The first is the aperture area, A, that determines the operating concentration ratio, defined as $C=\frac{P}{I \cdot A}$, where P is the operating power, measured at the aperture, and I=1 kW m^{-2} [7]. In the lab scale geometry this ratio was 2785 suns and to objectively assess the performance of the larger geometries more accurately, this ratio should remain at similar levels. In the scaled-up geometries, the aperture has a diameter of 0.37, 0.676, and 1.171 m, yielding a concentration ratio of 2790, 2786, and 2786 for the operating power of 0.3, 1, and 3 MW, respectively.

The mass of ceria and the shape of the RPC is the second important characteristic. To have a direct comparison between the different geometries, the RPC thickness remained fixed at 25 mm for every scale. To increase the mass load of ceria, the cavity was expanded by keeping the $\frac{Depth}{Width}$ ratio fixed and equal to the lab-scale geometry. Expansion continued until the ceria mass ratio between the large and small scale geometries was the same as the power ratio between the two, i.e.: $\text{mass}_{\text{CeO2-Large-scale}} = \frac{P_{Large-scale}}{3.5\ kW} \cdot \text{mass}_{\text{CeO2-3.5 kW}}$. The mass of the RPC for the investigated geometries, as well as the cavity characteristics, can be seen in Table 1. The material properties and RPC structure characteristics are assumed to be unaffected by the scaling-up process.

TABLE 1. The dimensions and ceria mass load of the studied scaled-up geometries.

Scale-Up Cases	Cavity Depth [m]	Cavity Width [m]	CeO_2 Mass [ton]
0.3 MW	0.825	1.1	0.145
1 MW	1.53	2.04	0.49
3 MW	2.67	3.56	1.478

The Al_2O_3 insulation surrounding the RPC had a fixed thickness of 0.17 m for all scaled-up cases. The resulted window, mounted on the front aluminum insulation with a height of 0.17 m, has a diameter of 0.71, 1.02, and 1.51 m in the 0.3, 1, and 3 MW geometries, respectively. Such a large window, subject to intense radiation on one side and sub-atmospheric and high-temperature conditions on the other, could suffer great mechanical stress and might be a limiting factor for large scale geometries. Consequently, optimized cooling techniques are required to reduce the thermal stress on the window. Finally, the entire reactor is enclosed by a 7 mm thick Inconel vessel. Specific scaling-up methodology for the insulation material was not considered and the presented dimensions consist in an initial estimate. Thicker or thinner insulation would affect the heating up and/or cooling down time of the reactor and should be addressed in combination with heat capture and recycle mechanisms in a plant design study.

The used scaling-up methodology is not an optimization for the large-scale geometries. Instead, it is useful as a direct comparison between the different scales that operate at the same conditions and as an indication of what scaling-up can provide for the studied geometry.

Scaling-Up Benefit

One reduction step was simulated with all geometries, including the lab-scale geometry, operated at nominal power. The pressure within the cavity for all cases was assumed as 1 mbar and Argon injection was not used, since in a fuel production plant, operating at lower P_{O2} to boost the O_2 release from ceria while minimizing the energy penalties due to inert gas consumption would be highly beneficial for the plant efficiency. Pressure levels below 1 mbar seem currently not realistic [15]. Reduction lasted until 1% of the RPC volume reached 2073 K, representing a maximum high-temperature limit for increased s-t-f energy conversion efficiency and yield while simultaneously respecting the physical and chemical stability limits of the material. The resulting efficiency is presented in Fig. 2a.

The 0.3 MW geometry outperforms the larger scale geometries, with the exception of the first few reduction minutes. Furthermore, the lab-scale geometry also reaches a higher s-t-f efficiency than the 1 and 3 MW geometries. These results are contrary to the expectation that the larger the scale, the higher the performance and the benefit will be. A deeper investigation is crucial to determine the reason for this behavior.

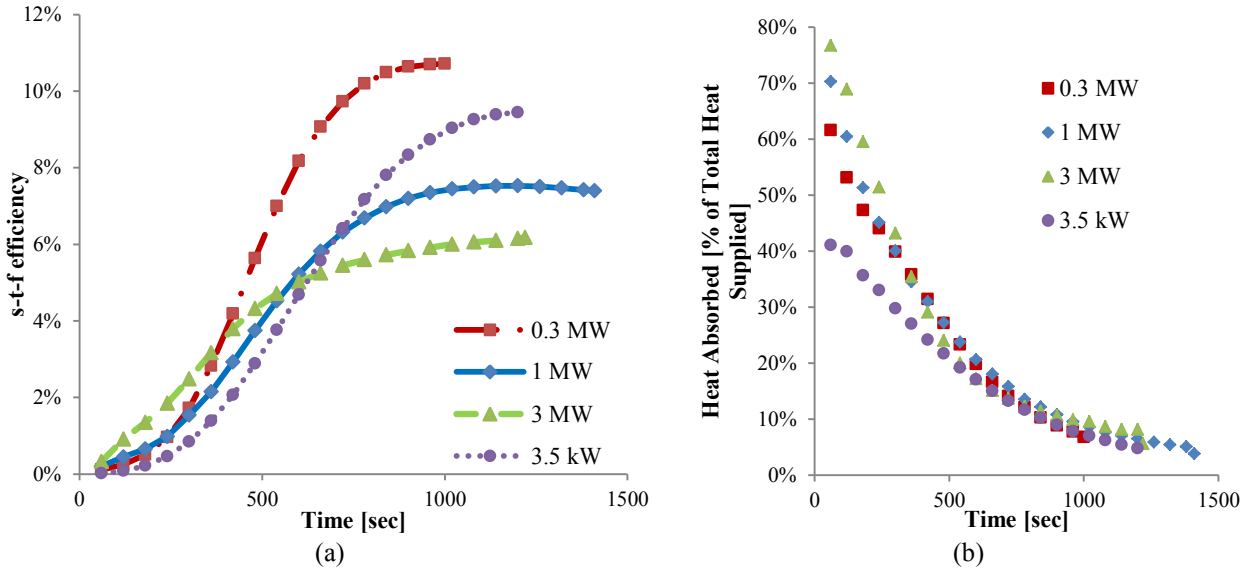

FIGURE 2. (a) The solar-to-fuel energy conversion efficiency of the different cases, operating at nominal power, 1 mbar pressure and no Argon injection. (b) The heat absorbed by the RPC, expressed as percentage of the total supplied heat during reduction.

The scaling-up methodology considers an increase in all dimension and operating ratios proportional to the scale-up magnitude. The constant $\frac{Depth}{Width}$ ratio in the cavity and the $\frac{P}{m}$ scale-up constraint ensured that the incident radiation absorbed by the irradiated ceria surface (kWm^{-2}) and the total heat per mass of ceria (Jkg^{-1}) would be quasi constant in the three large-scale geometries. This proportionality however was not enforced in the RPC thickness, result which significantly altered the heating-up behavior and the performance of the three scale-up cases in comparison with the lab-scale geometry. Specifically, the three large-scale geometries have a much lower ratio of power input to irradiated surface area, equal to 76.9±2 kWm^{-2}, compared to the lab-scale geometry, which was at 111.4 kWm^{-2}. This is a direct consequence of restricting the RPC thickness, instead of proportionally increasing it with the cavity, during the scaling-up process, since in order to keep the $\frac{P}{m}$ constraint, the large-scale cavity, and thus the irradiated surface, should expand further compared to a direct 1-to-1 scaling-up approach based on the lab-scale reactor. As a result, comparing the three large-scale geometries with the lab-scale results is inconclusive to evaluate the scale-up benefit. Instead, this benefit can be evaluated more precisely by comparing solely the performance of the three large-scale cases which share quasi-similar design and operational characteristics.

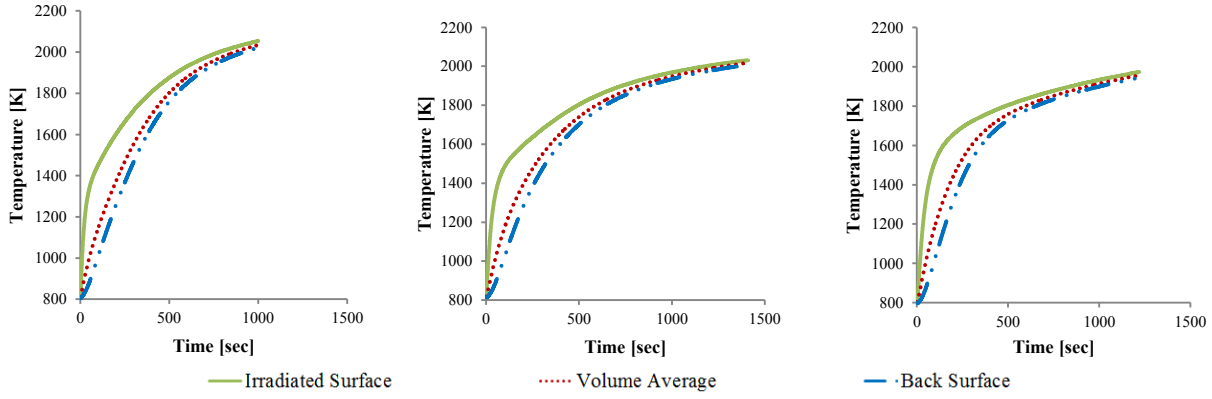

FIGURE 3. The average temperature evolution of the irradiated surface, volume and back surface of the RPC for the (a) 0.3, (b) 1, and (c) 3 MW cases, respectively.

The quasi-similar ratio of power input to irradiated surface area in the three large-scale geometries translates into a comparable heating-up rate in the irradiated RPC surface, seen in Fig. 3. Noticeably, the larger the reactor size, the higher the heat absorbed by the RPC, absorption which is expressed as the percentage of the total supplied heat to the reactor during the reduction step in Fig. 2(b). This heat absorption is used to heat up the deeper parts of the RPC and, in combination with a comparable heating rate in the irradiated surface for all three cases, translates into a much faster heating rate in the RPC volume and back surface at the two larger scales. Subsequently, temperature uniformity across the RPC volume is reached faster for each consecutive scale-up. While this behavior is desirable to minimize the thermal stress on the RPC, unfortunately it is also associated with a steady-state effect where the $\frac{dT}{dt}$ gradient is minimized, easily observable in the heating-up behavior of the 1 and 3 MW geometries. This gradient drives the reduction reaction, thus a steady-state is associated with saturation effect and limited O_2 production from the exhausted RPC. As a result, the performance of the larger reactors is hindered and the smaller geometries can outperform them. It is important to also notice the heating-up rate of the 0.3 MW case, which almost achieves the ideal behavior: a gradual heating rate of the RPC volume over the entire reduction duration, spending only a minimum amount of time in a steady-state. The smaller scale of this geometry possibly allows its RPC to still be within the acceptable thickness limits to avoid a saturated ceria volume.

Conclusively, steady-state effects should be considered in larger scale reactors and it is crucial for their performance to ensure that the implemented RPC is able to perform as expected, by achieving a gradual heating rate throughout its intended reduction duration. This becomes more pressing at each consecutive scale-up. Further improvements on the performance of the reactor should be mainly focused on design optimization and improved distribution of CeO_2 within the cavity. Design optimizations can be defined using a dedicated optimization tool. Improved CeO_2 distribution is possible through the implementation of a thin ceria layer on the conical Al_2O_3 section. This layer will protect the insulation from extreme temperatures while also increasing the total O_2 production, since the resulting temperature in the Al_2O_3 is high enough to drive the reduction reaction.

It should be mentioned again that the scaling-up methodology has the purpose of defining the benefit associated with scaling-up the solar reactor technology and should not be interpreted as a potential assessment of the different scales. It is evident from the performance of the 0.3 MW case that large-scale reactors have the potential for increased s-t-f energy conversion efficiency values but there are setbacks that should be avoided. The results presented in this paper can serve as a guideline for such restrictions as well as an indication for further reactor improvements and optimization.

Even though optimization of the solar reactor is crucial to achieve commercial implementation, it should be addressed in combination with a plant design study, as well as an economic and environmental impact study. As part of an interconnected system, the reactor has several different optimization possibilities, with each one affecting and being affected by the larger plant system. This potential plant system might have distinct goals, such as maximizing fuel production and/or environmental/economic impact, rather than maximizing the solar-to-fuel energy conversion efficiency of the reactor sub-system. Depending on the results of these studies, the reactor can be optimized for fast and flexible redox cycles or longer cycles with maximum O_2/Syngas yield per cycle, with different optimization methodologies examined for each case. For a plant simulation a more simplified model will be needed to analyze the reactor performance for different design and operational conditions with less computational effort. This would help

defining the optimum operational parameters for the reactor, which can be integrated in the validated 3D model for further optimization, detailed investigation during operation and addressing problematic instances in the reactor level.

CONCLUSIONS

The validated simulation of the solar reactor with a dual-scale RPC can capture the heating up and O_2 release trends, making it an important tool for the design of larger scale geometries, relevant in a fuel production plant. The simulated scaled-up geometries, equal to 0.3, 1 and 3 MW, display a higher solar-to-fuel energy conversion efficiency in the first few reduction seconds compared to the lab-scale design, but the restriction of the RPC thickness caused saturation and a steady-state effect which eventually hindered the performance of the larger scales. Optimizing the solar reactor is possible through the use of validated models, but optimization should be addressed in combination with a plant design and an economic/environmental impact study.

ACKNOLEDGEMENTS

This project has received funding from the European Union's Horizon 2020 research and innovation programme under grant agreement No 654408 // This work was supported by the Swiss State Secretariat for Education, Research and Innovation (SERI) under contract number 15.0330. This document reflects the authors' view only and the INEA must not be taken as responsible for any use that may be made of the information it contains.

REFERENCES

1. IPCC Fifth Assessment Report, "Climate Change 2014 Mitigation of Climate Change", Chapter 8: Transport.
2. H. Kuhn, C. Falter, A. Sizmann, "Renewable Energy Perspectives for Aviation", Proc. 3rd CEAS Air Conf. 21st AIDAA Congr. 2011, 1249-1259
3. European Commission, "A policy framework for climate and energy in the period from 2020 to 2030", Brussels, 22.1.2014
4. M. Takacs, S. Ackermann, A. Bonk, M. Neises-von Puttkamer, Ph. Haueter, J.R. Scheffe, U.F. Vogt, A. Steinfeld, "Splitting CO_2 with a Ceria-Based Redox Cycle in a Solar-Driven Thermogravimetric Analyzer", AIChE Journal, April 2017 Vol. 63, No.4
5. D. Marxer, P. Furler, M. Takacs, A. Steinfeld, "Solar thermochemical splitting of CO_2 into separate streams of CO and O_2 with high selectivity, stability, conversion, and efficiency", Energy Environ. Sci., 2017, 10, 1142-1149
6. S. Ackermann, M. Takacs, J. Scheffe, A. Steinfeld, "Reticulated porous ceria undergoing thermochemical reduction with high-flux irradiation", International Journal of Heat and Mass Transfer, Volume 107, April 2017, Pages 439-449
7. P. Furler, J. Scheffe, M. Gorbar, L. Moes, U. Vogt, A. Steinfeld, "Solar Thermochemical CO2 Splitting Utilizing a Reticulated Porous Ceria Redox System," Energy & Fuels, October, 2012 (11), 7051-7059
8. P. Parthasarathy, P. Le Clercq, "Heat transfer simulation in a high temperature solar reactor", SolarPACES 2014, Elsevier 2015
9. P. Parthasarathy, P. Le Clercq, "Numerical Simulation of Heat transfer in a 3D cavity-receiver," ASME, 2015.
10. P. Furler, J. Scheffe, D. Marxer, M. Gorbar, A. Bonk, U. Vogt and A. Steinfeld, "Thermochemical CO_2 splitting via redox cycling of ceria reticulated foam structures with dual-scale porosities", Phys. Chem. Chem. Phys., 2014,16, 10503-10511
11. ANSYS Inc. "ANSYS CFX-Solver Theory Guide", Release 15.0, November 2013
12. M. Kaviany, "Principles of Heat Transfer in Porous Media", 2nd ed., 1995, Springer, New York
13. R. Bader, L.J. Venstrom, J.H. Davidson, W. Lipiński, "Thermodynamic Analysis of Isothermal Redox Cycling of Ceria for Solar Fuel Production", Energy & Fuels 2013, 27(9), 5533-5544
14. Rath, "ALTRA®KVS HIGH-TEMPERATURE VACUUM-FORMED BOARDS AND SHAPES", DE 19711, 2017, http://www.rath-usa.com/kvs_high.php
15. S. Brendelberger, H.v. Storch, B. Bulfin, and C. Sattler, , "Vacuum pumping options for application in solar thermochemical redox cycles – Assessment of mechanical-, jet- and thermochemical pumping systems", Solar Energy, 141 (2017) 91-102.